Journal of Catalysis 310 (2014) 75–83

Contents lists available at ScienceDirect

Journal of Catalysis

journal homepage: www.elsevier.com/locate/jcat

A novel TiO_2 composite for photocatalytic wastewater treatment

Mohamed S. Hamdy [a,b], Wibawa H. Saputera [a], Edgar J. Groenen [c], Guido Mul [a,*]

[a] Photocatalytic Synthesis Group, MESA+ Institute for Nanotechnology, Faculty of Science and Technology, University of Twente, P.O. Box 217, 7500 AE Enschede, The Netherlands
[b] Chemistry Department, Faculty of Science, Helwan University, Cairo, Egypt
[c] Leiden Institute of Physics, Leiden University, Niels Bohrweg 2, 2333CA Leiden, The Netherlands

ARTICLE INFO

Article history:
Received 27 April 2013
Revised 14 July 2013
Accepted 16 July 2013
Available online 30 August 2013

Keywords:
Rutile
Anatase
Ti_2O_3
Methyl orange
Photocatalysis
Oxygen vacancies
Ti^{3+}
Composite
Electron transfer

ABSTRACT

A novel TiO_2 composite consisting of Anatase interacting with a Ti^{3+}-containing Rutile phase was synthesized by heating a mixture of TiO_2 (Hombikat) and Ti_2O_3 in air at different temperatures ranging from 300 °C up to 900 °C. The preparation of the samples was analyzed by Thermal Gravimetric Analysis (TGA), and the resulting composites characterized by X-ray powder diffraction (XRD), Raman and UV–Vis spectroscopy, X-ray Photoelectron Spectroscopy (XPS), Electron Paramagnetic Resonance (EPR) spectroscopy, and Scanning Electron Microscopy. Characterization data show a phase transformation from Ti_2O_3 to Ti^{3+}-containing Rutile at temperatures of around 600 °C. Moreover, Hombikat is gradually converted from amorphous to crystalline Anatase. The Ti^{3+}-content and the degree of Anatase crystallinity are respectively inversely and directly proportional to an increasing preparation temperature. The composite which was synthesized at 600 °C showed the highest photocatalytic rate in the decolorization of Methyl Orange (MO). The rate constant was significantly larger than obtained for Evonik P25 after identical thermal treatment (600 °C). Photodeposition of Pt further not only enhanced the photocatalytic activity of the optimized composite, but surprisingly also the stability. The methyl orange degradation results are discussed on the basis of hole and electron transfer phenomena between Anatase and Rutile phases, the latter containing (surface) oxygen vacancies (Ti^{3+}). The presence of surface oxygen vacancies and/or Pt nanoparticles is proposed to be of benefit to the rate determining oxygen reduction reaction.

1. Introduction

Heterogeneous photocatalysis is a promising technology for removal of organic pollutants from water and air. It has shown potential as an environmental friendly, low cost, and sustainable technology. TiO_2 is by far the most frequently applied photocatalyst. The photocatalytic activity and stability of TiO_2 are unprecedented in particular in wastewater treatment [1], in which organic compounds are totally converted into carbon dioxide and water [2,3]. It has often been reported that the Anatase phase of titania is the most active phase, whereas the effects of the simultaneous presence of Rutile (or Brookite) are still unclear [4–6]. Another aspect of TiO_2-based photocatalysis recently (re)addressed is the degree of reduction of the semiconductor [7]. Partially reduced titania crystals (TiO_{2-x}, where typically $0 < x < 1$) induce high photocatalytic rates in wastewater treatment [8,9], air purification [10], hydrogen production by water splitting [11,12], and selective oxidation in organic media [13]. However, the stability of Ti^{3+} centers, in particular if these are located on the surface, is generally low [13].

Several methods have been reported to create reduced titania crystals such as (i) plasma treatment [14], (ii) laser treatment [15], (iii) thermal treatment under vacuum, helium or hydrogen atmosphere [16,17], (iv) bombardment with high energy particles (e.g., neutrons [18], or γ-rays [19]), and (v) thermal treatment in CO and/or NO [12]. While of interest for fundamental studies, various of these methods are inconvenient for synthesis of large quantities of reduced TiO_2 required for practical applications.

Recently, Hashimoto et al. [20] reported a simple one-step synthesis procedure to prepare TiO_2 samples consisting of a stable Rutile phase in contact with Ti^{3+} containing Rutile by thermal treatment of a mixture of commercially available Rutile and Ti_2O_3 at elevated temperature (up to 900 °C). However, the observed photocatalytic performance of the prepared material in the gas-phase reaction of 2-propanol to acetone was negligible without co-catalyst (CuO nanoparticles [20]).

Here, we report on an adaption of the synthesis method of Hashimoto et al. [20], by changing Rutile for high surface area Anatase in the synthesis procedure. Furthermore, we have analyzed the composites in detail by various microscopic and spectroscopic techniques. The photocatalytic activity of the thus prepared catalysts at variable calcination temperature was evaluated in

* Corresponding author. Address: Photocatalytic Synthesis Group, MESA+ Institute for Nanotechnology, Faculty of Science and Technology, University of Twente, P.O. Box 217, 7500 AE Enschede, The Netherlands. Fax: +31 53 4892882.
E-mail address: G.Mul@utwente.nl (G. Mul).

0021-9517/$ - see front matter © 2013 Elsevier Inc. All rights reserved.
http://dx.doi.org/10.1016/j.jcat.2013.07.017

the aqueous-phase decomposition of Methyl Orange (MO). The obtained photocatalytic rates will be discussed on the basis of the characterization data: crystalline Anatase in close contact with partially reduced Rutile provides for the highest rates. In addition, photodeposition of Pt will be demonstrated to further enhance the catalytic rates, as well as the stability of the composite.

2. Experimental

2.1. Synthesis

A one-step synthesis procedure was applied to synthesize the composites. In a typical synthesis procedure, 1 g of commercial TiO_2 powder of the Anatase phase (Hombikat UV 100, Sachtleben Chemie GmbH) was mixed and grinded with 1 g of Ti_2O_3 (Aldrich, 99.9%). The mixed fine powder was heated at different temperatures from 300 °C to 900 °C for 3 h in static air applying a heating rate of 5 °C/min. Samples are labeled M-*x*, where *x* is the heating temperature. Furthermore, two reference samples of Ti_2O_3 heated at 600 °C for 3 h (Ti_2O_3-600) and a mixture of Rutile (Aldrich 204757-25G) and Ti_2O_3 were prepared in static air at 900 °C for 3 h, applying a heating rate of 5 °C/min.

Platinum was photo-deposited on the composite as follows: 200 mg of the M-600 composite was introduced into a top illumination reactor. Then, 23.7 ml of water, 26.3 ml of H_2PtCl_6 (2 wt.%), and 12 ml of methanol were added to the reactor, respectively. The solution was irradiated with UV light (Carl ZEISS, HBO 50W) for 24 h, during which the solution was sparged with a moderate air flow. After the irradiation process, the residue was centrifuged off at 8500 rpm for 10 min and then washed few times with distilled water until no chloride anion was detected by a silver ion test. The solution was dried overnight at 100 °C in a furnace. The thus produced powder is labeled Pt-M-600 throughout this paper.

2.2. Characterization

Thermal Gravimetric Analysis and Differential Scanning Calometry profiles were analyzed using a NETSZCH STA 449 F1 Jupiter instrument and 10 mg of the TiO_2/Ti_2O_3 composite. The temperature range under investigation was room temperature up to 900 °C, applying a heating rate of 5°/min under 20 ml/min flow of air or nitrogen, respectively.

The crystal structure of the samples was determined in air by X-ray Diffraction using a Bruker D2 phaser instrument. The samples were ground and sieved to obtain a fine powder of particle sizes <50 μm. Data were collected varying 2θ between 10° and 90° with a step size of 0.005°. The Anatase to Rutile ratio was estimated from the Spurr equation [21]:

$$X_R = 1.26I_R/(I_A + 1.26I_R)$$

X_R is the Rutile fraction and I_R and I_A are the strongest intensities in the Rutile ((110)) and Anatase ((101)) diffraction pattern, respectively.

Nitrogen physisorption measurements were carried out at 77 K with a Micromeritics Tristar system (ASAP 2400) to determine the textural properties. Prior to the adsorption measurements, the samples were degassed at 573 K and 10^{-3} Pa for 24 h. The specific surface areas were calculated according to the Brunauer–Emmet–Teller (BET) method.

Diffuse reflectance UV–Vis spectra were collected at ambient temperature on an EVOLUTION 600 (ThermoScientific) spectrometer, using $BaSO_4$ as reference. Spectra were recorded in the wavelength range of 200–800 nm.

Raman spectra were recorded using a Bruker Senterra Raman Spectrometer equipped with a N_2 cooled CCD detector (213 K). A green (λ = 532 nm) laser with intensity of 2 mW was used for excitation. Spectra were acquired at a resolution of 9 cm^{-1}, and 10 scans were accumulated for each spectrum.

X-ray photoelectron spectroscopic (XPS) analysis was performed using a Quantera SXM spectrometer made by Physical Electronics. The radiation was provided by a monochromatized Al Kα (1486.6 eV) X-ray source, operated at a 25 W emission power and a 15 kV acceleration voltage.

The presence of Ti^{3+} in various composites was also evaluated using EPR spectroscopy, using a Bruker Elexsys 680 instrument. The EPR measurement was conducted at 9.73 GHz (X-band). The microwave power was set at 2.526 mW, the modulation amplitude at 5G, and the temperature of measurement at 80 K.

The morphologies of the samples were investigated by scanning electron micrsocopy (SEM), using a HR-SEM-LEO 1550 equipped with NORAN EDS and WDS capabilities.

2.3. Catalytic activity

Photocatalytic activity measurements were carried out in a home-built reactor housing [22]. The housing consists of an aluminum box with dimensions of 60 cm in height, 600 cm in width, and 40 cm in depth, containing an electric fan for cooling and eight Philips black light tubes (F20 T8 BLB, 18W, 60 cm in length) for illumination. Each lamp can be independently controlled, with the emitted wavelength ranging from approximately 350 to 400 nm, and maximum intensity at 375 nm. The overall incident intensity of the light was 3.21 mW/cm^2 at the surface of the aqueous catalyst/dye composition contained in open glass beakers (height 8 cm, volume 100 ml), which were used as reactors. The catalyst suspension was continuously agitated by magnetic stirring, and air delivery with a rate of 20 ml/min.

The photocatalytic activity of the prepared materials was tested in the decolorization reaction of Methyl Orange (MO). In a typical reaction, 50 mg of the catalyst was introduced into a beaker containing 50 ml of MO (20 mg/L). The suspension was ultra-sonicated for approximately 10 min and then placed into the reactor. Once in the reactor housing, the solutions were stirred for 30 min in the dark at room temperature to allow for complete chemisorption. Once this time had elapsed, a sample of the solution was taken, and the remaining reaction solution irradiated with UV light. Additional samples were taken every 20 min, filtered through a 0.2-mm PTFE Millipore membrane filter to remove suspended catalyst agglomerates, and finally analyzed using a UV–Vis spectrometer (EVOLUTION 600 (ThermoScientific)) in the range between 250 and 600 nm to determine the concentration of the dye.

The reaction rate constant (k_a) was then determined assuming *quasi* first order kinetics using the following equation:

$$\ln(C_0/C) = k_a t$$

where C_0 is the concentration of the dye in solution after chemisorption, C is the concentration at time t, and k_a is the reaction rate constant. All reactions were repeated at least two times with fresh catalyst. The standard deviation was estimated to be ±5%.

In one case, the air supply was replaced for N_2 (20 ml/min) to identify the necessity of O_2 for the dye decomposition reaction. In another experiment, the black light tubes were exchanged for similar Philips tubes with emission ranging from 435 to 475 nm, and maximizing at 455 nm. This to evaluate the visible light induced activity of the optimized catalyst composition (in the presence of air delivery).

Catalyst stability was evaluated as follows: a catalyst composite was filtered after use, washed several times with distilled water, and finally dried at 100 °C for 24 h in static air. Re-suspension in fresh dye solution was followed by the steps indicate above for

the fresh catalyst samples. Catalysts were used up to as much as three times.

3. Results

3.1. Thermal analysis of a physical mixture of Hombikat/Ti_2O_3

The thermal analysis of a mixture of Hombikat and Ti_2O_3 is shown in Fig. 1. Under nitrogen flow, there is only a small increase in sample weight at high temperature, while major heat effects are absent (not shown). This small increase is probably related to oxidation of Ti_2O_3 by small quantities of O_2 present in the nitrogen environment (the oven was not absolutely gas tight). However, under oxygen flow, oxidation causes a significant weight increase from ~400 °C upwards. The exothermic DSC signal maximizing at 610 °C signals the oxidation of Ti_2O_3 to TiO_2. It should be noted that the oxidation process is not complete at 700 °C. A slow, but continuous increase in weight up to 900 °C can be observed. This increase in weight at high temperatures suggests slow oxidation of remaining reduced domains (presumably oxygen vacancies) in the interior of the formed Rutile crystals. When the TGA experiment is complete at 900 °C, the sample has gained approximately 5% in weight, which is in good agreement with the theoretical conversion of Ti_2O_3 to TiO_2 (5.6% given a ratio of 1:1 of Ti_2O_3:Hombikat in the sample, and a total sample weight of 12 mg).

3.2. Chemical composition of the composites

The XRD patterns of the Hombikat/Ti_2O_3 composites obtained after calcination at different temperatures are presented in Fig. 2 and compared to the patterns of the parent materials. The pattern of Hombikat is characterized by broadened reflections at 26.0°, 38.5°, and 48.6° 2θ, in agreement with an Anatase phase of poor crystallinity. Commercial Rutile shows reflections around 28.2° and 36.8° 2θ, while Ti_2O_3 is characterized by reflections around 24.6°, 33.6°, and 35.6° 2θ. After calcination at relatively low temperatures, the reflections of the parent Hombikat and Ti_2O_3 can still be identified. Above 400 °C, the diffraction pattern of the Ti_2O_3 phase vanishes, whereas diffraction lines of Rutile appear, clearly demonstrating the transformation of Ti_2O_3 into Rutile at calcination temperatures above 400 °C (in agreement with the TGA analysis). The observed temperature of conversion of the Ti_2O_3 phase into Rutile is in good agreement with a recently reported study of Kako et al. [23]. In the pattern of the M-600 sample, the diffraction lines of Anatase (Hombikat) become more intense and sharp, an indication of increasing degree of crystallinity of the Anatase phase. In the pattern of the M-900 sample, the Anatase phase is still present, indicating a high resistance of the Anatase phase to transform into Rutile. The Anatase/Rutile ratio was calculated from the Spurr equation and is shown as a function of calcination temperature in Fig. S1. The fraction of Rutile increases as a function of increasing heating temperature up to 600 °C, after which the Rutile to Anatase ratio is relatively constant. This is entirely caused by the transformation of Ti_2O_3 into Rutile, in agreement with the TGA analysis. The final molar ratio of Anatase/Rutile equals 2:1, in agreement with an initial ratio of Anatase/Ti_2O_3 of 1:1, and the following reaction:

$$2Ti_2O_3 + O_2 \rightarrow 4TiO_2 \text{ (Rutile)} \quad (1)$$

Raman spectroscopy confirmed the compositional changes as observed by XRD (Fig. 3). Ti_2O_3 displays weak Raman bands, in agreement with the study of Kako et al. [23]. The spectrum of the M-300 sample exhibits bands at 392, 513 and 635 cm^{-1}, which are characteristic of the Anatase phase of TiO_2 [24]. Two additional

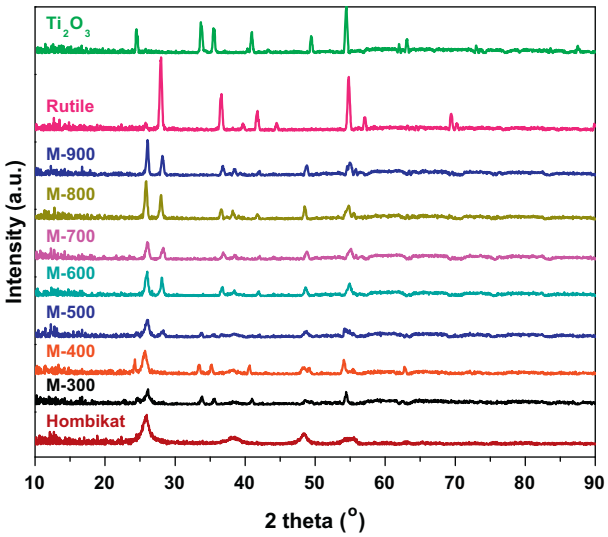

Fig. 2. XRD patterns of the as prepared composites compared to patterns of Hombikat, Rutile and Ti_2O_3 as references, clearly demonstrating the transformation of Ti $_2O_3$ into Rutile at temperatures above 400 °C. Diffraction lines of Anatase sharpen, indicative of increasing crystallinity of the Hombikat Anatase phase.

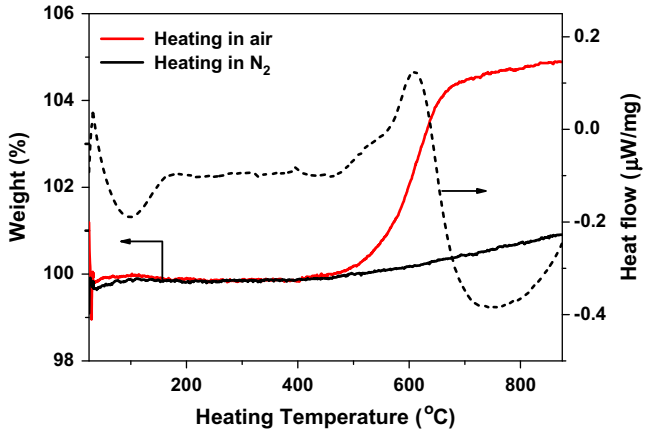

Fig. 1. TGA profiles of TiO_2 (Hombikat)/Ti_2O_3 (1:1 weight ratio) heated in air and in nitrogen atmosphere. The initial sample weight was approximately 20 mg.

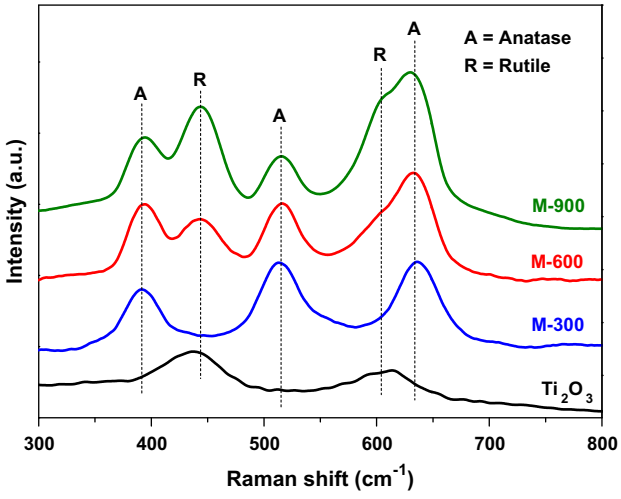

Fig. 3. Raman spectra of the prepared composites, as compared to the Ti_2O_3 spectrum. All spectra were collected at ambient conditions.

bands at 443 and 610 cm^{-1}, characteristic of the Rutile phase, develop comparing the spectra of M-600 and M-900. In agreement with the TGA and XRD data, Ti_2O_3 is oxidized at elevated temperature in air and converted to Rutile starting from ~400 °C.

XPS analysis was carried out to investigate the surface oxidation state of titanium in various composites. In general, a $Ti2p_{3/2}$ signal (or shoulder) at 457.8 eV can be assigned to surface Ti^{3+}, while a peak at 459.1 eV is attributed to Ti^{4+} containing compounds [25,26]. Fig. 4 shows the XPS standard binding energy of $Ti2p_{3/2}$ of the samples M-300, M-600, and M-900. From the spectra, it can be concluded that the amount of surface Ti^{3+} decreases in the series M-300 > M-600 > M-900. This is again consistent with the phase transformation of Ti_2O_3 into Rutile [23] and with data reported by Kako et al. [23]. We would like to state, however, that the detection limit for Ti^{3+} in XPS is in the order of ~0.5 wt.%, and we cannot exclude the presence of remaining surface defect sites after treatment at elevated temperature. This will be further discussed in relation to the observed photocatalytic activity data.

EPR spectroscopy was used to identify the presence of Ti^{3+} in the bulk structure of the composites (Fig. 5). The *g* factor of the composites are listed in Table 1 and compared to the *g* factors of Ti_2O_3. Paramagnetic Ti^{3+} centers show an EPR signal at $g = 1.974$ [27]. From the spectra, we can thus conclude that M-300 contains paramagnetic Ti^{3+}, although the EPR signals are significantly smaller as compared to the parent Ti_2O_3. This is predominantly the result of dilution of Ti_2O_3 by Hombikat TiO_2 in the M-300 sample. The EPR signal of M-600 shows significant broadening as compared to M-300. This broadening is the result of transformation of Ti_2O_3 into a Rutile phase containing oxygen vacancies. This is confirmed by comparison of the EPR spectra of the composite M-600 to Ti_2O_3 treated at similar temperature (600 °C, see Fig. S2). The two spectra are almost identical. In the EPR spectra of the composite treated at 900 °C (M-900), still some paramagnetic centers are present, albeit in minor quantities as compared to M-600. This indicates that some oxygen vacancies remain even at 900 °C (probably mostly in the interior of the Rutile crystal). The observations are in excellent agreement with the slow weight increase at high temperatures as observed in the TGA experiment.

UV–Vis spectra of M-300, M-600 and M-900, collected at ambient conditions, are shown in Fig. 6. The spectra demonstrate changes in light absorption characteristics, in agreement with color changes from gray to yellow to white (Fig. S3). The pale gray M-300 shows an absorption band with an onset at 370 nm in the UV range, typical for Hombikat Anatase. Furthermore, absorption is apparent over the entire range of 400–600 nm, slightly increasing

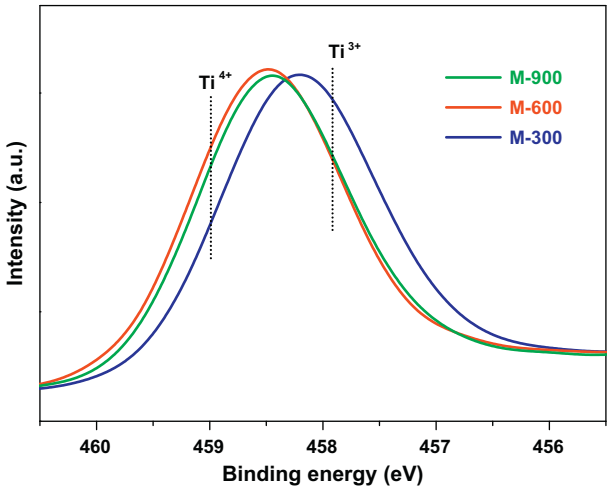

Fig. 4. The XPS $Ti2p_{3/2}$ spectra of M-300, M-600, and M-900 composites.

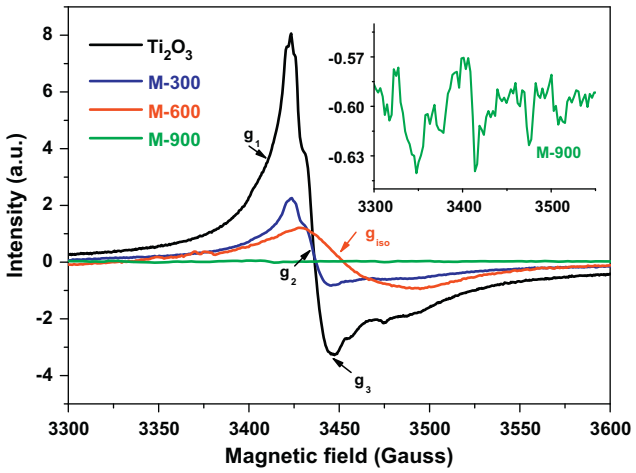

Fig. 5. EPR spectra of M-300, M-600, and M-900 composites compared to the Ti_2O_3 spectrum. Inset: EPR spectrum of M-900.

Table 1
Values determined for the *g* factors in commercial Ti_2O_3, M-300, and M-600.

Samples	*g*-factor
Ti_2O_3	$g_1 = 1.986$ $g_2 = 1.974$ $g_3 = 1.968$
M-300	$g_1 = 1.986$ $g_2 = 1.974$ $g_3 = 1.968$
M-600	$g_{iso} = 1.966$

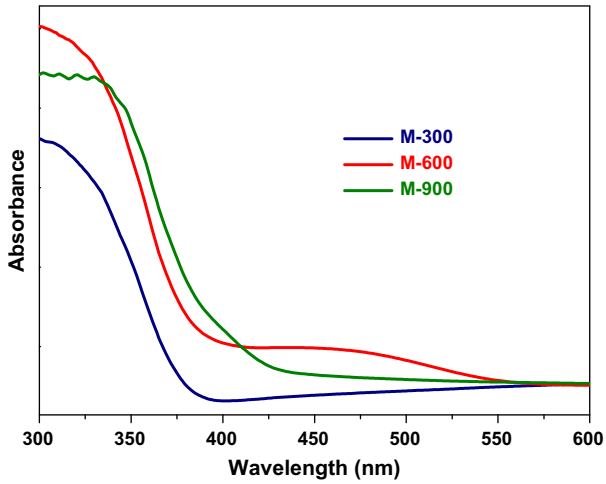

Fig. 6. UV–Vis spectra of M-300, M-600, and M-900. The spectra were collected at ambient conditions.

as a function of increasing wavelength, and related to the presence of Ti_2O_3. In the yellow M-600 composite, intensities in the visible-light range significantly increase between 400 and 550 nm. Based on the XRD, XPS and EPR analysis described above, we assign this (broad) visible absorption to the formation of a Rutile phase by conversion of Ti_2O_3, containing oxygen vacancies (associated with the presence of Ti^{3+}). The broad absorption range is no longer apparent in the spectrum of the off-white M-900 composite. A shoulder on the characteristic Anatase absorption band can be observed in the 400–450 nm range, indicative for the presence of

Rutile. The absorption spectra of the composites are in good agreement with those presented in the work of Kako et al. [23].

3.3. Morphology of the composites

Fig. 7 – Left panel presents the N_2 sorption isotherms of the different prepared samples compared to the original Hombikat sample. The isotherms are changing from type VI to type III according to IUPAC classification, i.e., changing from a mesoporous to a microporous structure. This result is in-line with the XRD results which indicate an increasing degree of crystallinity of the composite as a function of increasing calcination temperature. The BET surface area decreases sharply as a function of calcination temperature, in agreement with earlier studies (Fig. 7 – right panel) [28].

HR-SEM images of M-300, M-600, and M-900 are presented in Fig. 8. The Ti_2O_3 crystals are obviously visible in the M-300 composite and surrounded by the Hombikat (agglomerated) nanoparticles. In the M-600 composite, the Ti_2O_3 crystals are phase-transformed to peculiar-shaped crystals (appearing to have a fish-skin-like structure). As a function of increasing calcination temperature, the crystal boundaries become less sharp and less clear (i.e., partially fused) in M-900, consistent with the slightly lower intensity of the Rutile phase reflections in XRD, and explaining the calculated decreasing Rutile phase fraction in the composites (Fig. S1). Moreover, Hombikat becomes more crystalline, but is still present as a separate (Anatase) phase. Significant physical interaction seems to be present between the two phases in the composites.

3.4. The photocatalytic behavior of the composites

The photocatalytic activity of the TiO_2/Ti_2O_3 composites synthesized at different temperatures was evaluated in the decolorization reaction of Methyl Orange (MO). When Ti_2O_3 is heated at different temperatures (600–900 °C), the samples do not exhibit any photocatalytic activity in MO dye decomposition. Similarly, composites derived from Rutile/Ti_2O_3 mixtures calcined at different temperatures neither exhibit significant photocatalytic activity (see Fig. S4). These results are in agreement with observations by Hashimoto et al. [20], who concluded that the composite formed by heating Rutile with Ti_2O_3 at 900 °C has no activity without a co-catalyst (copper), albeit in the gas-phase reaction of isopropanol to acetone. Contrary, the Hombikat TiO_2/Ti_2O_3 composite samples showed considerable photocatalytically activity (Fig. 9). The

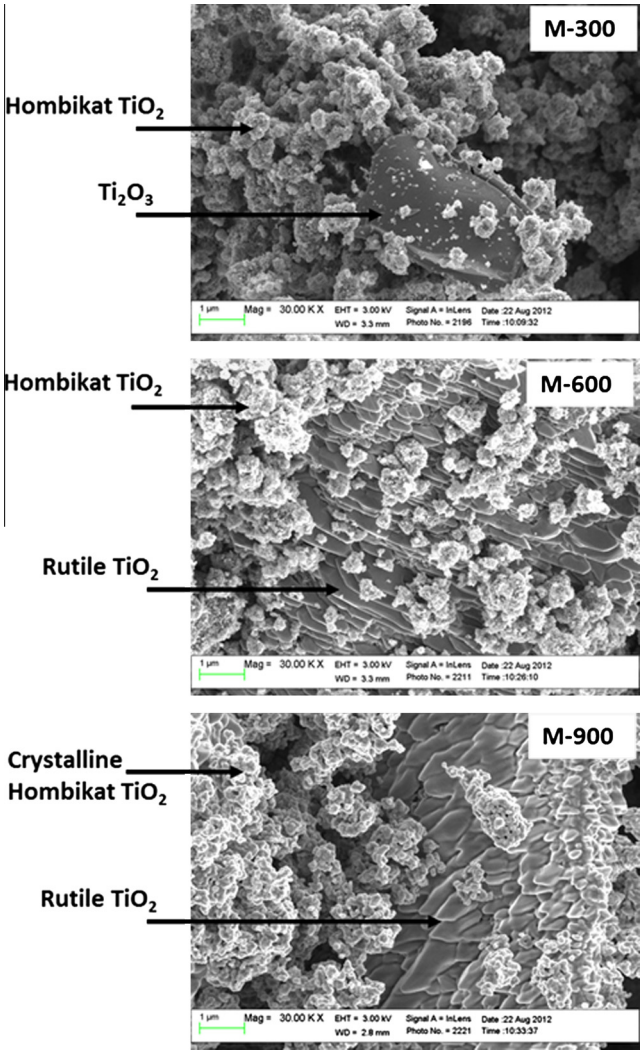

Fig. 8. HR-SEM micrographs of M-300 (top), M-600 (middle), and M-900 (bottom).

M-600 sample is the most active sample and exhibits higher photocatalytic activity than Hombikat or P25, thermally treated at 600 °C under identical conditions. A detailed comparison of the

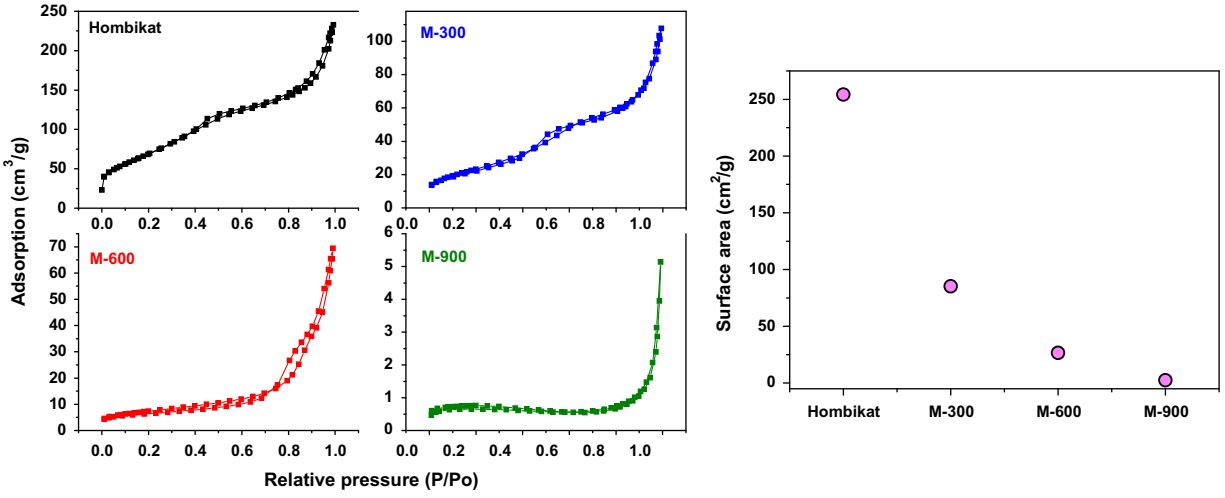

Fig. 7. Left panel: The N_2 sorption isotherms of M-300, M-600, and M-900 compared to TiO_2 (Hombikat). Right panel: The corresponding BET surface areas.

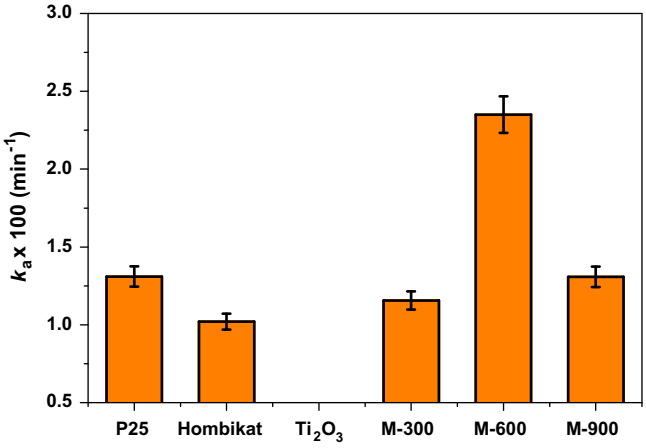

Fig. 9. The apparent first-order rate constant (k_a) of the decolorization of MO. Please note that the Hombikat and P25 samples were thermally treated at the optimized temperature of the composites, i.e., 600 °C. The rate constant has not been corrected for changes in surface area (Fig. 7).

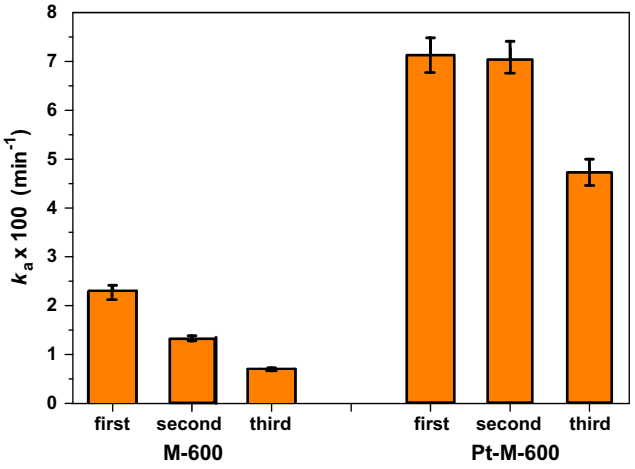

Fig. 11. A comparison between the apparent first order rate constant (k_a) of M-600 and Pt-M-600 up to the 3rd run.

various samples as a function of calcination temperature is provided in Fig. S5. The apparent photonic efficiency ranges from 1% for Hombikat to 4% for the most effective composite. Obviously, the presence of an Anatase phase and a partially reduced Rutile phase in the composite leads to improved synergy in the photocatalytic processes as compared to the P25 composition (also consisting of Rutile and Anatase phases). The apparent 1st order rate constants (k_a) of samples with different initial Hombikat/Ti_2O_3 ratio prepared at 600 °C are summarized in Fig. 10. The catalytic activity maximizes at an initial molar ratio of 1:1 (and final Anatase/Rutile ratio of 2:1). Unfortunately, the catalytic stability of such composite was poor: a loss in activity of approximately 65% was observed in a third consecutive experiment (Fig. 11).

The photocatalytic behavior of the optimized composite can be further enhanced by addition of a co-catalyst. To this end, the M-600 sample was functionalized by photodeposition of 2 wt.% platinum. The morphology of Pt in the composite was addressed by HR-SEM, combined with EDX analysis. Pt nanoparticles of high dispersion and sizes in the range of 5–10 nm can be observed (Fig. 12). The photocatalytic activity of the platinized sample (Pt-M-600) was almost three times higher than of M-600 (Fig. 11). Surprisingly, the stability of Pt-M-600 is also significantly larger than of M-600. The Pt functionalized composite shows a loss of only 30% in activity in a third run as compared to the fresh sample.

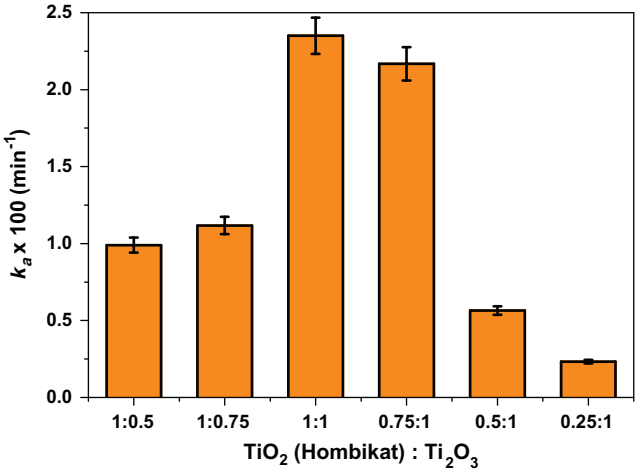

Fig. 10. The apparent first-order rate constant (k_a) of composites with different ratio synthesized at 600 °C.

4. Discussion

4.1. Characterization data

The composition and photocatalytic behavior of composites originating from thermally oxidized Ti_2O_3 [23] and a combination of thermally oxidized Ti_2O_3 and TiO_2 (Rutile) have been described in the literature previously [20]. Generally, the characterization data of thermally treated Ti_2O_3 reported in our study are in agreement with those reported in [20,23]. TGA analysis, XRD patterns, Raman spectra, UV/Vis data, and XPS spectra all demonstrate the conversion of Ti_2O_3 into Rutile, containing more or less oxygen vacancies, depending on the temperature of thermal treatment. EPR spectroscopy demonstrates the presence of these oxygen vacancies (Ti^{3+}) even after temperature treatment as high as 900 °C. It should be noted that the interpretation of the observed small EPR signals requires further in depth analysis and is beyond the scope of this paper. It finally should be noted that we cannot exclude the presence of surface oxygen vacancies. We propose some oxygen vacancies still to be present on the surface, which is necessary to explain the various catalytic phenomena (see following paragraph).

Summarizing the characterization data, the composites (as a function of treatment at increasing temperatures) consist of two separated phases of titania: Anatase of increasing crystallinity originating from Hombikat, and an oxygen vacancy containing Rutile phase originating from Ti_2O_3. The amount of oxygen vacancies (Ti^{3+}) is decreasing as a function of increasing preparation temperature, likely from the outside inwards. A schematic representation of the structures is presented in Fig. 13.

4.2. Photocatalytic activity

The composites prepared show significant activity in the decomposition of methyl orange. In should be noted that the apparent 1st order rate constant (k) reported for P25 in this study is comparable to values reported in the literature, as shown in Table 2. While comparing photocatalytic rates is not straight forward, since the reactor, light source, and intensity entering the reactor are often different in various studies (contributing to the spread

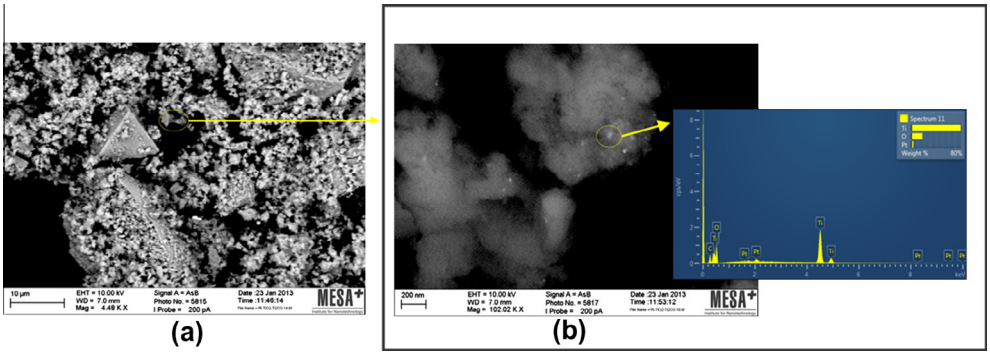

Fig. 12. HR-SEM micrograph of the Pt-M-600 sample. Inset: The EDX analysis.

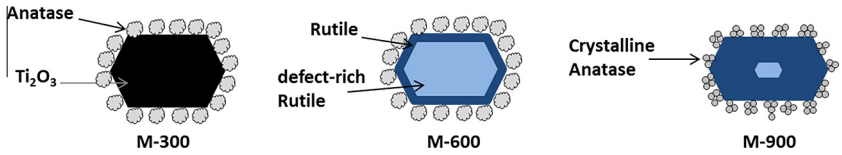

Fig. 13. Schematic diagram of the prepared composites. The irregular shape of Anatase represents the initial porous and agglomerated character, converted in crystalline phase (small circular particles). Black Ti_2O_3 is converted to Rutile, with a gradually decreasing concentration of bulk and surface defect sites as function of increasing calcination temperature.

Table 2
The apparent 1st order rate constant (k_a) reported for (calcined) P25 in this study as compared to values reported in the literature.

MO concentration	P25 concentration (g/l)	Reactor	Light source	k (min^{-1})	Source
0.0125 mM	Thin film		Black light tubes, 18 W	0.83×10^{-3}	Duta et al. [29]
25 ppm	0.83 g/l	Suspension	Black light tubes, 30 W	4.36×10^{-3}	Wang et al. [30]
0.05 mM	2.5 g/l	Suspension	UV lamps	7.5×10^{-3}	Carreon et al. [31]
0.018 mM		Suspension	UV tube, 6 W	6.2×10^{-3}	Zhang et al. [32]
0.15 mM	2 g/l	Suspension	UV lamp 15 W	15×10^{-3}	Peng et al. [33]
0.03 mM	1.25 g/l	Suspension	UV tube, 15 W	5×10^{-3}	Fu et al. [34]
0.06 mM	1 g/l	Suspension	UV lamp, 8 W	2.8×10^{-3}	Wang et al. [35]
0.03 mM	1 g/l	Suspension	Black light tubes, 18 W	7×10^{-3}	Du et al.[a]
0.06 mM	1 g/l[b]	Suspension	Black light tubes, 18 W	11×10^{-3}	This study

[a] Unpublished data.
[b] Calcined P25.

in the *k*-values reported in the literature), it is obvious that the rate constants of the composites determined in the present study are significantly higher than what has been previously reported for P25. Our composites containing Anatase are also significantly more active than catalysts obtained by Ti_2O_3 calcination, or calcination of Rutile/ Ti_2O_3 composites. Kako et al. [23] report the highest activity of Ti_2O_3 in 2-propanol oxidation (1000 ppm in air) when thermally treated at 700 °C in air. This catalyst was exposed to visible light in the wavelength range of 400–530 at an intensity of 5 mW cm^{-2} (reactor surface 8.5 cm^2). Contrary, Hashimoto et al. [20] observed no activity in the same reaction (300 ppm 2-propanol in air), when using a similar irradiation source (but now at 1 mW cm^{-2}, and reactor surface of 5.5 cm^2), unless thermally treated Ti_2O_3 was functionalized with Cu(II) oxide. The differences in performance between these studies are not obvious to explain, but our data appear to agree with the data of Hashimoto et al. [20], even though the reaction conditions are quite different (gas-phase 2-propanol oxidation *vs.* UV-stimulated aqueous-phase dye degradation). Even when exposed to UV light, the thermally treated Ti_2O_3 (resulting in low surface area Rutile) is not active in dye degradation, irrespective of the calcination temperature. However, contrary to a lack in activity of thermally treated Rutile/Ti_2O_3 composites in isopropanol oxidation upon visible light activation [20], Anatase/Ti_2O_3 composites showed extraordinary activity in aqueous-phase MO dye degradation when albeit to light with wavelengths of 375 nm, and activity, all be it lower, is even significant exposing the composite to 455 nm (Fig. S6). We will discuss the high performance on the basis of the following considerations.

4.3. The Anatase to Rutile ratio

The excellent activity of our composites consisting of Anatase and Rutile phases is in agreement with the extensively reported synergetic effect of these two phases in the literature (usually used to explain the high activity of P25). However, understanding the synergy between the two phases in *non*-trivial. Upon UV light activation, the presence of Rutile is often proposed to improve lifetimes of photo-excited states in the Anatase phase, induced by transfer of photo-excited holes from the Anatase to the Rutile phase. The valence band maximum of Rutile is higher in energy than of Anatase [36], energetically favoring such hole transfer. Such effect has recently been confirmed by Time Resolved Microwave Conductivity (TRMC) measurements [37], showing increased levels of conductivity and electron lifetimes in mixtures of Rutile and Anatase, as compared to the individual phases. Whether this phenomenon leads to enhancement in rates is depending on the rate determining step, i.e., oxygen reduction (on the Anatase phase) or hole transfer to hydroxyl groups. In case of the former,

a higher rate will be obtained for Anatase–Rutile composites; in case of the latter, a negative influence of the hole transfer phenomenon might be expected. This is based on the following reasoning. After being transferred to the Rutile phase, the holes need to initiate formation of OH radicals (or oxidation of adsorbed dye molecules) on the Rutile particles. However, the amount of OH groups on the Rutile surface is often far less as compared to Anatase, and evidence exists that Anatase-related OH groups are dominant in catalyzing dye oxidation [38]. This also comes into agreement with the dependency of the reaction rate constant with the Anatase surface hydroxyl group concentration previously reported for methylene blue degradation [39]. It should be noted that the likely negative effect of the presence of Rutile (in case OH radical formation is limiting) in composites is often over-compensated by improved morphological properties of the Anatase phase in such composites. The photoconductivity and electron lifetimes increase with increasing particle size and crystallinity of the Anatase phase, increasing the probability of effective oxygen reduction. An optimized calcination temperature of Hombikat for aqueous-phase dye-degradation reactions was previously determined at ~600 °C [38].

Given the higher activity of P25 as compared to Hombikat in our process conditions, we suggest that the oxygen reduction reaction is likely rate limiting. Consequently, the presence of the hole transfer from Anatase to Rutile is likely to contribute to the very high apparent rate constant for the composite M-600. If oxygen reduction is limiting, one would expect a deterioration in rate when oxygen is (partially) removed from the reaction mixture. This is confirmed by the experiment reported in Fig. S6, although significant conversion remains in the absence of oxygen. The latter suggests a substantial fraction of MO decomposition is caused by reaction with hydroxyl radicals formed by hydroxide oxidation, while photo-excited electrons are likely transferred to protons in anaerobic conditions, forming hydrogen. Besides the synergy between Rutile and Anatase phases, an additional property contributes to the high activity of the M-600 composite, to be discussed in the following.

4.4. The role of oxygen vacancies

The presence of surface oxygen vacancies, associated with Ti^{3+}, seems to also positively affect the activity of the composite upon UV activation. Kako et al. [23] explain the highest activity of Ti_2O_3 calcined at 700 °C by an optimum concentration of oxygen vacancies: oxygen vacancies are responsible for enhanced visible light absorption (positive), but also serve as recombination centers of electron–hole pairs (negative). Hashimoto et al. [20] discuss the energy diagram of Rutile TiO_2 containing interstitial sites, proposing these act as electron donors. The EPR and UV/Vis spectra (Fig. 6) confirm the presence of these sites in the composites, which is also in agreement with the (low) visible light activity obtained (Fig. S6, left). Equally important, however, is the presence of surface oxygen vacancies. As stated previously, due to detection limits, the absence of a clear Ti^{3+} signature in the XPS analysis does not exclude these surface vacancies to be present, which provides for a reasonable explanation of the enhanced activity of the M-600 composite as compared to P25. These vacancies likely act as reactive sites for oxygen reduction (or proton reduction in anaerobic conditions). We thus speculate the additional activity of the composite is related to photo-excited electron transfer steps to O_2 occurring efficiently at these vacancies. The photo-excited electrons might originate from Rutile-based light absorption, or alternatively from Anatase excitation, followed by transfer to the surface defect sites on the Rutile phase. Evidence that both excited electron sources are contributing is provided by an experiment evaluating visible light activity of the M-600 composite (Fig. S6, right). Photocatalytic activity is clearly present and has to be the result of (oxygen vacancy containing) Rutile-based light absorption (Anatase does not absorb light at 445 nm). At the same time, the activity is significantly higher at 375 nm, suggesting photo-excited electrons in the Anatase phase are largely contributing to activity, possibly after transfer from the Anatase to the Rutile phase.

Unfortunately, the formed superoxide anions not only react with (adsorbed) dye molecules, but also restore the surface vacancies, presumably in a stoichiometric fashion. Thus, the deactivation of the M-600 composite can be explained. Interestingly, after 3 cycles, the remaining activity is even lower than P25. To explain this, it can be speculated that the Anatase–Rutile interaction is not as intense in M-600 as in commercially available P25, and therefore, hole and/or electron transfer between phases less efficient. Hole and/or electron transfer are/is likely necessary to achieve synergy. The higher activity induced by Pt, as well as the higher stability, is discussed in the following paragraph.

4.5. The effect of Pt promotion

Hashimoto et al. [20] observed a necessity to promote thermally treated Rutile/Ti_2O_3 composites with CuO to obtain photocatalytic activity. An optimized Rutile/Ti_2O_3 ratio of 1:1 of the CuO promoted composite was reported and an optimized calcination temperature of 900 °C [20]. We also observed an optimized ratio of Anatase/Ti_2O_3 ratio of 1:1, while the thermally treated Anatase/Ti_2O_3 composite displayed highest activity when calcined at a temperature of 600 °C. The activity of the optimized composite was significantly improved by the addition of Pt particles. The beneficial effect of Pt nanoparticles on photocatalysts active in dye degradation is well known and has been extensively reported in the literature. Generally, these metal nanoparticles are claimed to decrease electron–hole recombination by transfer of photo-excited electrons from the semiconductor to the metal. In addition, Pt is an excellent oxygen reduction catalyst. We follow these propositions to explain the enhancement in activity of our composites. Presumably, Pt is present both on the Anatase and Rutile phases. Clearly, the Pt particles on the Anatase phase have a similar promoting effect as reported for catalysts consisting of pure Anatase. At the same time, the catalytic function of the oxygen vacancies (Ti^{3+}) in the Rutile phase might also be promoted by the presence of Pt.

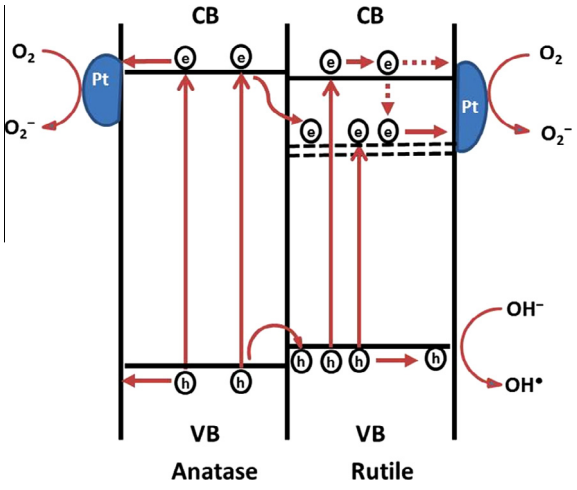

Fig. 14. Scheme of the proposed electron and hole transfer processes explaining the high photocatalytic activity of the Pt-M-600 composite. The various steps are extensively described in the main text.

What has not been reported previously in the literature is the beneficial effect of Pt nanoparticles on the stability of the composite (i.e., the oxygen vacancies). Two explanations present themselves: (i) due to the presence of Pt particles on the Anatase phase, less electrons are transferred to the Rutile phase, necessary for oxygen reduction and reaction with the vacancies, and (ii) the vicinity of the Pt particles to the vacancies on the Rutile phase prevents re-oxidation by preferred oxygen adsorption (and reaction) over these Pt nanoparticles. Currently, we have no preference for one of these two options, and both might actually be relevant.

5. Conclusions

Catalyst composites made by heating a mixture of Anatase/Ti_2O_3 showed very high photocatalytic activity in dye decolorization. Characterization results show that the composites exist of crystalline Anatase interacting with a well-defined Rutile phase containing bulk and surface oxygen vacancies, the quantity of which is depending on calcination temperature. The composite heated at 600 °C with an initial ratio of Anatase/Ti_2O_3 of 1:1 exhibits the highest photocatalytic efficiency. Photodeposition of Pt on the composite not only improves the photocatalytic performance, but also enhances the catalytic stability of the composite. The hole and electron transfer phenomena we believe are relevant to explain the high activity of the composites are schematically shown in Fig. 14: (i) hole transfer from Anatase to Rutile promotes the oxygen reduction reaction on the surface of Anatase, (ii) the oxygen vacancies on the Rutile surface promote oxygen reduction by electrons transferred from the Anatase phase, (iii) Pt promotes oxygen reduction on the Anatase and Rutile surfaces, and (iv) Pt decreases both electron transfer from the Anatase phase to the Rutile phase, and oxygen adsorption on the Rutile-associated oxygen vacancies, thereby increasing the photocatalytic stability of the composite.

Acknowledgments

W.H. Saputera thanks the University of Twente Scholarship (UTS) program and the Indonesian Ministry of National Education for his personal fellowship. The authors thank Mrs. F. Nami (Leiden University) for performing the EPR measurements. Mr. G. Kip, Mrs. L. Vrielink, and Mr. R. Veneman (Twente University) are acknowledged for recording XPS spectra, and conducting N_2 physisorption, and TGA measurements, respectively.

Appendix A. Supplementary material

Supplementary data associated with this article can be found, in the online version, at http://dx.doi.org/10.1016/j.jcat.2013.07.017.

References

[1] M.N. Chong, B. Jin, C.W.K. Chow, C. Saint, Water Res. 44 (2010) 2997–3027.
[2] A.L. Linsebigler, G. Lu, J.T. Yates, Chem. Rev. 95 (1995) 735–758.
[3] A. Fujishima, T.N. Rao, D.A. Tryk, J. Photochem. Photobiol. C 1 (2000) 1–21.
[4] K. Tanaka, M.F.V. Capule, T. Hisanaga, Chem. Phys. Lett. 187 (1991) 73–76.
[5] T. Ohno, K. Sarukawa, M. Matsumura, J. Phys. Chem. B 105 (2001) 2417–2420.
[6] T. Ohno, K. Sarukawa, M. Matsumura, New J. Chem. 26 (2002) 1167–1170.
[7] L.B. Xiong, J.L. Li, B. Yang, Y. Yu, J. Nanomater. 2012 (2012).
[8] M. Xing, W. Fang, M. Nasir, Y. Ma, J. Zhang, M. Anpo, J. Catal. 297 (2013) 236–243.
[9] Z. Zheng, B. Huang, J. Lu, Z. Wang, X. Qin, X. Zhang, Y. Dai, M.-H. Whangbo, Chem. Commun. 48 (2012) 5733–5735.
[10] I.N. Martyanov, T. Berger, O. Diwald, S. Rodrigues, K.J. Klabunde, J. Photochem. Photobiol. A 212 (2010) 135–141.
[11] X. Chen, L. Liu, P.Y. Yu, S.S. Mao, Science 331 (2011) 746–750.
[12] F. Zuo, L. Wang, T. Wu, Z. Zhang, D. Borchardt, P. Feng, J. Am. Chem. Soc. 132 (2010) 11856–11857.
[13] M.S. Hamdy, R. Amrollahi, G. Mul, ACS Catal. 2 (2012) 2641–2647.
[14] J. Zhang, Q. Xu, Z. Feng, M. Li, C. Li, Angew. Chem. 120 (2008) 1790–1793.
[15] T. Le Mercier, J.M. Mariot, P. Parent, M.F. Fontaine, C.F. Hague, M. Quarton, Appl. Surf. Sci. 86 (1995) 382–386.
[16] V.E. Henrich, R.L. Kurtz, Phys. Rev. B 23 (1981) 6280–6287.
[17] H. Liu, H.T. Ma, X.Z. Li, W.Z. Li, M. Wu, X.H. Bao, Chemosphere 50 (2003) 39–46.
[18] T.-C. Lu, L.-B. Lin, S.-Y. Wu, C.-P. Zhao, X.-C. Xu, Y.-F. Tian, Nucl. Instrum. Meth. B 191 (2002) 291–295.
[19] S. Dohshi, M. Anpo, S. Okuda, T. Kojima, Top. Catal. 35 (2005) 327–330.
[20] M. Liu, X. Qiu, M. Miyauchi, K. Hashimoto, Chem. Mater. 23 (2011) 5282–5286.
[21] R.A. Spurr, H. Myers, Anal. Chem. 29 (1957) 760–762.
[22] M.S. Hamdy, E. Scott, R. Carr, J.M. Sanders, Catal. Lett. 142 (2012) 338–344.
[23] T. Kako, N. Umezawa, K. Xie, J. Ye, J. Mater. Sci. 48 (2013) 108–114.
[24] J. Zhang, M. Li, Z. Feng, J. Chen, C. Li, J. Phys. Chem. B 110 (2005) 927–935.
[25] R. Li, H. Kobayashi, J. Guo, J. Fan, Chem. Commun. 47 (2011) 8584–8586.
[26] Y.C. Lee, Y.P. Hong, H.Y. Lee, H. Kim, Y.J. Jung, K.H. Ko, H.S. Jung, K.S. Hong, J. Colloid Interface Sci. 267 (2003) 127–131.
[27] M. Xing, J. Zhang, F. Chen, B. Tian, Chem. Commun. 47 (2011) 4947–4949.
[28] J.T. Carneiro, A.R. Almeida, J.A. Moulijn, G. Mul, Phys. Chem. Chem. Phys. 12 (2010) 2744–2750.
[29] Radu Adrian Carcel, Luminita Andronic, Anca Duta, J. Nanosci. Nanotechnol. 11 (2011) 9095–9101.
[30] S. Wang, Q. Gong, J. Liang, Ultrason. Sonochem. 16 (2009) 205–208.
[31] A. Katti, S.R. Venna, M.A. Carreon, Catal. Commun. 10 (2009) 2036–2040.
[32] H. Zhang, R. Hou, Z. Lu, X. Duan, Mater. Res. Bull. 44 (2009) 2000–2008.
[33] N. Liu, Y. Zhao, X. Wang, H. Peng, G. Li, Mater. Lett. (2013), http://dx.doi.org/10.1016/j.matlet.2013.03.106.
[34] C. Tian, Q. Zhang, A. Wu, M. Jiang, Z. Liang, B. Jiang, H. Fu, Chem. Commun. 48 (2012) 2858–2860.
[35] Y. Wang, Z-H. Jiang, F-J. Yang, Mater. Sci. Eng. B 128 (2006) 229–233.
[36] R. Katoh, A. Huijser, K. Hara, T.J. Savenije, L.D.A. Siebbeles, J. Phys. Chem. C 111 (2007) 10741–10746.
[37] J.T. Carneiro, T.J. Savenije, J.A. Moulijn, G. Mul, J. Phys. Chem. C 115 (2011) 2211–2217.
[38] P. Du, A. Bueno-Lopez, M. Verbaas, A.R. Almeida, M. Makkee, J.A. Moulijn, G. Mul, J. Catal. 260 (2008) 75–80.
[39] J.T. Carneiro, T.J. Savenije, J.A. Moulijn, G. Mul, J. Phys. Chem. C 114 (2010) 327–332.